Results on Physical Constants and Related Data from the Radio Tracking of Mariner (Venus) and Ranger III–VII Missions

WILLIAM L. SJOGREN* AND DONALD W. TRASK†
Jet Propulsion Laboratory, California Institute of Technology, Pasadena, Calif.

The "real-time" flight-path analysis and performance are described for Ranger VI and VII missions. Over a large region of injection points for a Ranger mission, the midcourse maneuver can be based on an orbit with a 10–30km uncertainty‡ in the impact parameter B plane. The main problem in orbit determination is to obtain verification of data consistency between stations. As Ranger VI results show, small errors can perturb the orbit well beyond the 1-sigma target uncertainties. The Ranger VII photographs demonstrated that the impact point agreed to within 3 km. The predicted and observed impact times agreed to within 0.1 sec. The doppler measurements gave a real-time verification that the maneuver execution errors on Ranger VI and VII were well within design specifications. Determination of physical constants from earth-based radio tracking has resulted in improved knowledge of the mass of the moon of one order of magnitude and a factor of 4 for the earth. Station locations can be determined to 10 m in the radial direction normal to the earth's spin axis and in longitude differences to 20 m. The lunar radius at the impact points was determined to ±0.3 km and in both cases was found to be approximately 3 km less than the previously accepted value.

Introduction

THE series of Ranger flights to the moon and the Mariner II flight to Venus and beyond have provided precise radio tracking data that have contributed fundamental new experimental information concerning some of the important constants used to determine the mechanics of the solar system. Such improvement in our knowledge of these constants represents a valuable contribution and stimulus to the field of celestial mechanics and supplies graphic proof of the high-accuracy performance of earth-based radio tracking and guidance.

This paper reviews the Ranger and Mariner II missions from a tracking standpoint. The real-time flight-path analysis and the performance experienced during Ranger VI and VII missions are discussed in terms of the "correctness" of real-time orbit determination estimates and the execution errors of the midcourse maneuver. The orbit-determination accuracies that may be obtained during a Ranger mission are presented along with examples of how uncertainties in some of the physical constants limit the navigation accuracy.

Next, the results of the determination of physical constants from earth-based radio tracking of the Mariner II and the Ranger III through VII missions are presented. Analysis completed to date has allowed improvement of an order of magnitude in the knowledge of the mass of the moon and a factor of 4 for the earth. Information was also obtained on tracking station locations and the lunar radius at the Ranger VI and VII impact points.

The last section discusses the role of earth-based radio guidance (EBRG) for the Mariner IV, Surveyor, and the Apollo missions.

Presented as Preprint 65-91 at the AIAA 2nd Aerospace Sciences Meeting, New York, N. Y., January 25–27, 1965; revision received May 18, 1965. This paper presents the results of one phase of research carried out at the Jet Propulsion Laboratory, California Institute of Technology, under Contract No. NAS 7-100, sponsored by the National Aeronautics and Space Administration. The authors are grateful for additional analysis and support given by D. Curkendall, W. Kirhofer, D. L. Cain, T. W. Hamilton, J. Anderson, G. Null, K. Young, A. Liu, M. Warner, M. Nead, R. Holzman, D. Chaney, W. Wollenhaupt, and J. Carnakis.

* Senior Research Engineer, Orbit Determination Group, Systems Analysis Section.

† Group Supervisor, Orbit Determination Group, Systems Analysis Section.

‡ All statistics quoted in this paper are 1-sigma-value uncertainties unless otherwise stated.

Discussion

Data

The EBRG activities for a Ranger mission are carried out in the Space Flight Operations Facility (SFOF) at the Jet Propulsion Laboratory (JPL), Pasadena. Tracking data are received in near real-time at the SFOF from the Air Force Eastern Test Range (AFETR) and from the Deep Space Instrumentation Facility (DSIF). These data are then analyzed, the spacecraft orbit and related trajectory parameters are determined, and the maneuver requirements are computed by the Flight-Path Analysis and Command (FPAC) team.

The principal tracking data utilized to determine the Ranger post-injection orbit are provided by the DSIF. The three DSIF locations (Goldstone, Calif.; Johannesburg, South Africa; and Woomera, Australia) are illustrated in Fig. 1, along with their visibility regions, as a function of spacecraft altitude. The detailed characteristics of these stations may be obtained from Ref. 1.

The DSIF tracking data utilized to determine a Ranger orbit consist of angles (hour angle and declination) and two-way doppler. The angle data are valuable during the early portion of the flight, when the trajectory geometry is varying rapidly. However, beyond the first pass of Johannesburg (approximately injection plus 13 hr), the information gained by the continued use of angle data is overshadowed by that provided by two-way doppler. The two-way doppler is a

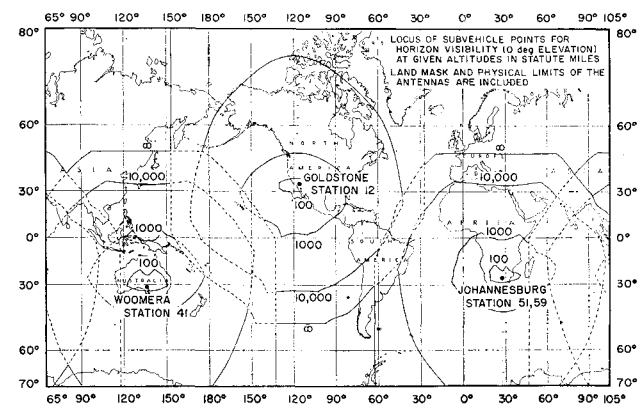

Fig. 1 DSIF location and visibility.

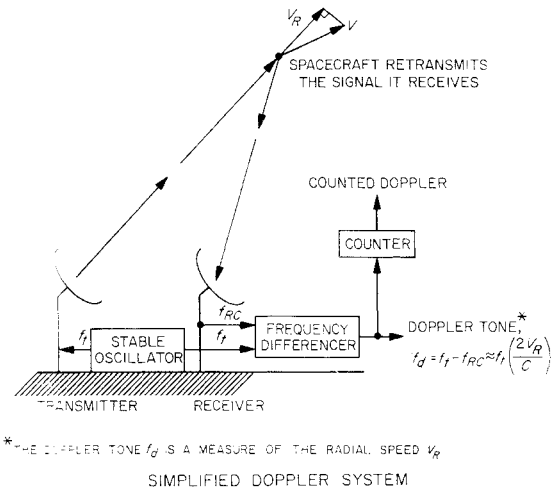

Fig. 2 Simplified two-way doppler configuration.

measure of the radial velocity V_R of the spacecraft relative to a tracking station. A simplified two-way doppler configuration is depicted in Fig. 2. The tracking station transmits a signal to the spacecraft. The signal received at the spacecraft is shifted in frequency by the well-known doppler effect. The spacecraft then retransmits the signal that it has received. The signal received at the ground receiver has been further doppler-shifted by the radial velocity of the receiver with respect to the spacecraft. The difference between the received frequency and the current transmitter frequency is called the doppler tone.

In practice, the doppler tone is continuously counted, and this continuous count is sampled from once a second to once a minute. The 1-sample/min mode is utilized over the majority of the flight, whereas the higher sample rates are used near injection, at lunar (planet) encounter, and during spacecraft maneuvers. These continuous-count doppler-tone samples are differenced to obtain a data type known as counted two-way doppler that is actually the range difference that occurred during a sample interval. By combining such doppler measurements taken over an interval of time at several stations, the spacecraft orbit may be reconstructed and its future course accurately predicted.

The AFETR net provides tracking data in the form of angles (azimuth and elevation) and ranges from launch through the early postinjection phase. These tracking data are obtained from a transponder on the Agena stage of the Atlas-Agena launch vehicle rather than the spacecraft and thus only supply approximate data on the spacecraft orbit once separation from the Agena stage has occurred shortly after injection. The AFETR provides pointing information and predictions of the doppler tone for the first pass of the spacecraft over the DSIF South African and Australian stations. The AFETR tracking data are also processed by JPL in near real-time to back up the AFETR prediction and orbit computations and as a consistency check on the early DSIF tracking data. The backup computations are made mainly to establish confidence in the quality of the AFETR and DSIF data.

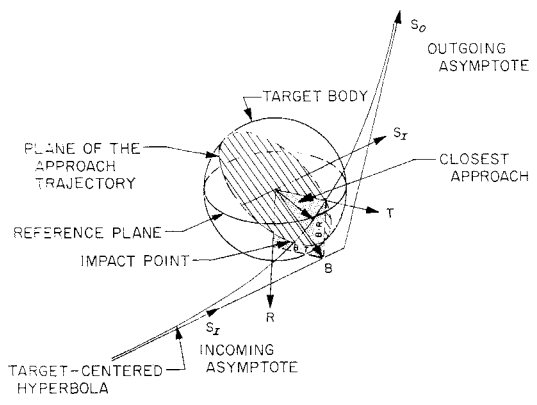

Fig. 3 Definition of $B\cdot T$, $B\cdot R$ system.

Coordinate System

The estimated spacecraft orbit and the quality of the estimate are generally expressed in the same type of target-centered coordinate system used by physicists to describe the bombardment of atoms by particles. This system, called the B-plane system, is defined in Fig. 3. The B-plane contains the center of the target body and is perpendicular to the incoming asymptote of the target-centered hyperbolic spacecraft orbit. The direction of this asymptote is denoted by the unit vector S and is the direction of the incoming hyperbolic excess velocity. The miss parameter B is a vector defined by the intersection of the B-plane and the plane of the spacecraft orbit relative to the target body. The components of the B-vector in the B-plane are described by the use of two unit vectors R and T such that T is taken parallel to a fixed reference plane and R, S, T form a right-handed orthogonal system. The orbit estimate is then expressed in terms of $B\cdot T$, $B\cdot R$, and flight time, whereas the statistics associated with the estimate are expressed in terms of the semimajor axis (SMAA) and the semiminor axis (SMIA) of the 1-sigma uncertainty ellipse in the B-plane plus the uncertainty of the flight time.

Examples of the use of the B-plane during a mission are presented in Figs. 4 and 5. The lunar surface has been mapped into the B-plane in Fig. 4. The acceptable zones for television pictures for the Ranger VII launch date are also shown. There are two advantages in presenting this type of chart in the B-plane system. First, it adequately describes trajectories that miss the target body as well as those that impact the target body; and second, a mapping to the B-plane of errors in the spacecraft orbit or the effects of a midcourse maneuver is relatively linear. Similar mappings to the lunar surface can be quite nonlinear, especially for a grazing impact trajectory. Figure 5 shows the capability of the midcourse motor to alter the spacecraft orbit as a function of time from launch. Nominally, a midcourse maneuver is performed near launch $(L) + 17$ hr for a Ranger mission, where the maneuver capability can correct for errors on the order of 5 sigmas in the launch-vehicle guidance system. In the event of a larger inaccuracy of the spacecraft injection by the launch vehicle or of a deterioration in the spacecraft midcourse maneuver capability (such as a leak in the fuel system), an early maneuver can take advantage of the increased effectiveness of the midcourse motor illustrated in Fig. 5.

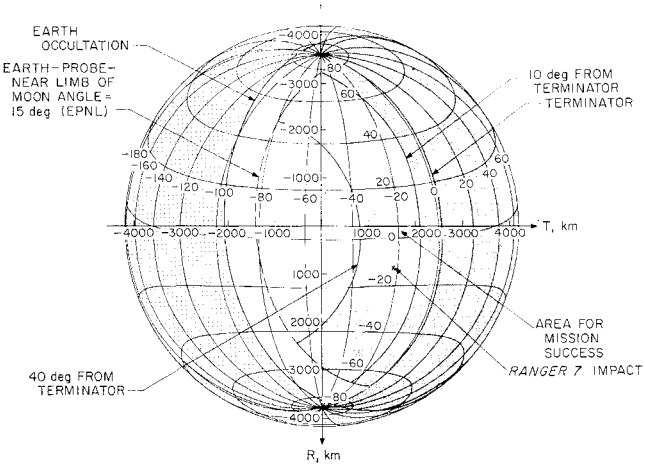

Fig. 4 Lunar surface with constraints in the B-plane Ranger VII.

Table 1 Ranger impact results

Mission	Impact location: Calculated: Lat., deg Long., deg	Impact location: Calculated: 1 σ, km Lat. 1 σ, km Long.	Impact location: Photographs: Lat., deg Long., deg	Impact location: Photographs: 1 σ, km	Impact time: Calculated: GMT, sec	Impact time: Calculated: 1 σ, sec	Impact time: Recorded: GMT, sec	Impact time: Recorded: 1 σ, sec	Remarks: 1 deg on lunar surface $\approx$ 30 kæ
Ranger 6	9.44/21.50 ($R_{\mathbb{C}}$ = 1735.32 km)	1.2/0.2	...	...	31.82	0.15	31.86	0.025	ΔAim lat. = +24 km, ΔAim long. = +12 km 1.5-sec residual with $R_{\mathbb{C}}$ = 1738.32 km
Ranger 7	−10.70/−20.67 ($R_{\mathbb{C}}$ = 1735.60 km)	1.0/0.2	−10.62/−20.59	3.0	48.74	0.19	48.80	0.025	ΔAim lat. = +9.0 km, ΔAim long. = +9.0 km

Flight-Path Performance during Ranger Missions

The Ranger VI and VII flights serve as dramatic demonstrations of EBRG capability. The best estimates of the Ranger VI and VII impact locations as determined from postflight analysis of the DSIF tracking data are shown in Table 1. These best estimates show that Ranger VI landed only 27 km from the target point and Ranger VII within 13 km.

There is little that is more satisfying in the field of orbit determination than to predict an event such as lunar impact and have the event happen exactly as predicted. The impact time for Ranger VI was predicted to within 1.5 sec of the actual occurrence. During postflight analysis, it was determined that a reduction in the lunar radius of approximately 3 km at the Ranger VI impact point was the most plausible way of eliminating this discrepancy. Consequently, during the Ranger VII mission, the estimate of the impact time was based on lunar radius 3 km less than that indicated by the Air Force Aeronautical Chart and Information Center (ACIC) lunar charts. This estimate was based on DSIF tracking data up to 2 hr before impact and was within 0.1 sec of the actual impact time as recorded by the loss of signal at the DSIF tracking stations.

The television pictures provide another check on the validity of the estimate of the Ranger VII orbit. The current best estimate of the Ranger impact point as determined from the television pictures is 3 km from that determined by the DSIF tracking data. Figure 6 shows the Ranger VII lunar track and the track of the optical axis of the various cameras as well as the area of the lunar surface effectively photographed by the television cameras. Also shown are the impact points as determined by the television pictures and by the DSIF tracking data. The provisional 1-sigma uncertainty associated with the television picture estimate is 3.0 km, whereas SMAA = 1.0 km on the lunar surface for the DSIF tracking data estimate.

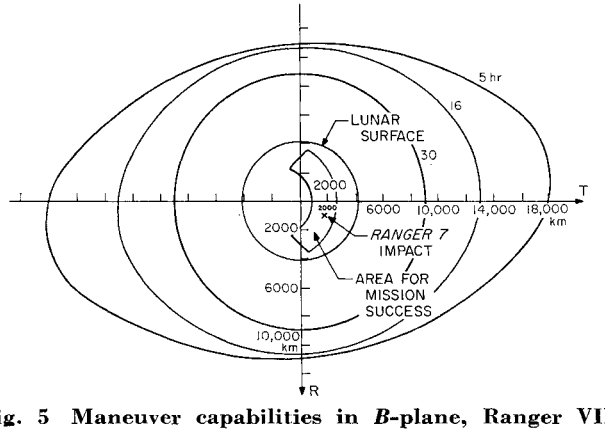

Fig. 5 Maneuver capabilities in *B*-plane, Ranger VII.

Using the postflight best estimates of the Ranger VI and Ranger VII orbits as a standard for comparison, the accuracy of the real-time orbit determination estimates, the performance of the midcourse maneuver and the performance of the launch vehicle can be rated quantitatively.

A measure of the actual quality of the real-time orbits as well as the inflight predicted quality is depicted in Table 2 for Ranger VI and Ranger VII. The inflight results are compared to the current best estimate of the orbit as determined from a postflight analysis of the DSIF tracking data. Notice that the actual quality of the Ranger VII real-time orbits exceeded the predicted quality, whereas the quality of the early real-time Ranger VI orbits is worse than the inflight estimated quality. This was caused by irregularities in the tracking data that are discussed later in this section.

The statistics (SMAA) quoted in Table 2 depend on the estimated parameters and on the noise characteristics of the data. The abbreviation STD. 6 in the "Code" footnotes of these tables stands for standard 6 (i.e., the six orbital elements; in this case, the three geocentric space-fixed position and three velocity components at an epoch). To be rigorous, pertinent physical constants such as tracking station locations and the mass of the earth should be included in the solution vector to obtain a true value of SMAA. However, this roughly doubles the required computing time and has a negligible effect, if the SMAA is greater than 50 km. Therefore, as an expediency, most of the premidcourse and early postmidcourse inflight orbits are computed with only the orbital elements in the solution vector. The values of the SMAA presented in Table 2 assume that the tracking data are good in the sense that the tracking data noise is caused only by the a priori expected error sources. A concerted effort is expended during a mission to check the consistency of the track-

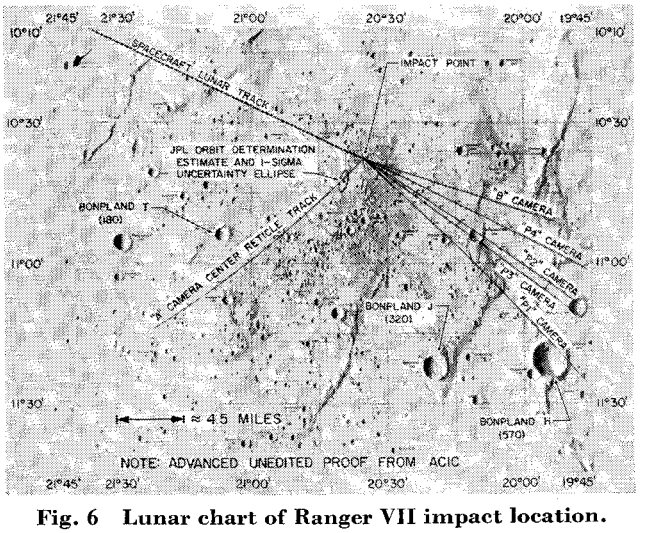

Fig. 6 Lunar chart of Ranger VII impact location.

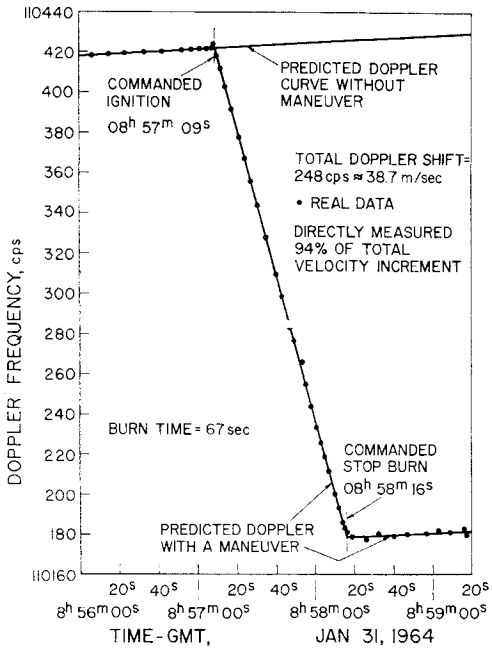

Fig. 7 Doppler during maneuver, Ranger VI.

ing data to ensure that this is the case. Two significant areas of inconsistent data were detected during the Ranger VI operation. The trouble was diagnosed, and the data were rejected. However, postflight analysis showed the true cause for the anomalies to be different from that suspected in flight, and this had resulted in some bad data being used in the real-time orbits.

The first data anomaly was an incorrect transmitter frequency that was reported during the first pass over the DSIF station in South Africa. It was realized in flight that some of the data were bad during this 26-min station tracking pass, and a decision was made in flight to use only the data from a 4-min interval. The rest of the data obtained during this pass were rejected. It was not until the postflight data analysis that the error in transmitter frequency was uncovered, and it was realized that the data accepted in flight were actually bad, whereas those previously considered inaccurate were actually good.

The second data anomaly was an 0.008-sec time bias at the DSIF station in Australia. This timing bias affected the doppler residuals for the early data. It was assumed in flight that these data had been corrupted by procedures related to switching from the acquisition aid antenna to the 85-ft main dish. Therefore, the data obtained in the first 10 min were rejected from the data set used in the real-time orbits. Again, it was not until the postflight data analysis that the 0.008-sec timing bias was uncovered as having existed throughout the Ranger VI flight. Together, these two data anomalies account for the major portion of the discrepancies noted in Table 2 between the inflight orbits and the current best estimate of the premidcourse orbit for Ranger VI.

The Ranger VI mid-course maneuver computations were based on tracking data from two stations: South Africa and Australia. Even after the "suspect data" had been rejected, a further family of orbits, which was run to check the tracking data, indicated that inconsistencies still existed. However, the variations in these orbits were well within the accuracy requirements of the project; therefore, the maneuver was executed as scheduled. The midcourse maneuver parameters and a division between the errors associated with the orbit determination process and the maneuver execution errors caused by hardware tolerances are shown in Table 3 for Rangers VI and VII. Notice that in Ranger VI a relatively large $\Delta B \cdot R$ error caused by *OD* was partially cancelled by a maneuver execution error. The Ranger VI *OD* errors were caused mainly by the irregularities in the early DSIF tracking data discussed previously. The *OD* errors are the differences between the inflight orbit on which the maneuver was based (as shown in Table 2) and the postflight best estimate of the premidcourse orbit. The maneuver error is the difference between the spacecraft orbit that would have been obtained, if the maneuver velocity increments had been applied to the best estimate of the premidcourse orbit and the actual orbit based on the best estimate of the postmidcourse orbit. The midcourse execution errors were well below the expected errors for both Rangers VI and VII. The *OD* errors were double those expected for Ranger VI but a fraction of those expected for Ranger VII (Table 2).

The radial component of the midcourse velocity increment is observed by the DSIF in real-time as a shift in the doppler tone. The comparison between the predicted and the actual doppler shift is shown in Fig. 7 for the Ranger VI midcourse maneuver. The difference between the predicted and the total doppler shift was 5 parts out of 10^5 or a magnitude less than the expected error in the maneuver radial velocity increment.

Orbit Determination Capabilities for Ranger Missions§

This section discusses the orbit-determination accuracies obtainable during the premidcourse and the postmidcourse

Table 2 Ranger VI and VII orbit determination results[b]

Time, hr	$\Delta B \cdot T$, km	$\Delta B \cdot R$, km	ΔT_F, sec	SMAA, km	Code[a]
Ranger 6 pre-maneuver					
$L + 2$[c]	−3000.0	4400.0	3020.0	2000.0	*A*
$L + 2.5$	−89.0	134.0	12.0	92.0	*A*
$L + 4$	−174.0	134.0	92.0	58.0	*A*
$L + 8$	−3.0	102.1	7.0	50.0	*A*
$L + 12$	−12.4	78.7	14.5	31.0	*A*
$L + 15$	−17.0	98.1	18.0	19.0	
Postmaneuver					
$M + 10$[c]	−57.0	82.0	9.0	71.0	*B*
$M + 22$	−45.0	47.0	16.0	52.0	*B*
$M + 35$	12.0	0.0	12.0	30.0	*C*
$M + 45 = I - 5$	4.0	30.0	3.0	28.0	*C*
$I - 1$[c]	−3.0	−4.0	1.5	21.0	*C*
Observed					
Ranger 7 pre-maneuver					
$L + 2$	170.0	31.0	414.0	1000.0	*D*
$L + 2.5$	21.0	89.0	−43.0	500.0	*E*
$L + 4$	6.0	3.0	−13.0	72.0	*F*
$L + 8$	1.0	18.0	−5.0	20.0	*F*
$L + 12$	6.0	13.2	−11.8	15.0	*G*
$L + 15$	3.0	19.0	−17.5	14.0	*G*
Postmaneuver					
$M + 10$[c]	9.0	−10.0	7.0	56.0	*C*
$M + 22$	0.0	7.0	3.0	34.0	*C*
$M + 35$	−1.0	4.0	0.0	25.0	*C*
$M + 45 = I - 5$	0.0	1.0	0.0	18.0	*C*
$I - 1$[c]	1.0	−1.0	0.0	15.0	*C*
Observed	4.0	4.0	1.5[d]		*H*

[a] Code defined as follows: *A* = STD. 6, doppler and angles; *B* = STD. 6, doppler only; *C* = STD. 6, plus $GM_{\odot}$, $GM_{\mathbb{C}}$, sta. loc., doppler only; *D* = STD. 6, 30 pts.; *E* = STD. 6, 2 stations, 80 pts.; *F* = STD. 6, 3 stations, doppler only; *G* = STD. 6, plus sta. loc.; and *H* = impact location "observed" by TV camera (0.5 km uncertainty).

[b] In-flight estimate minus current best estimate; tracking only.

[c] *L* = launch, *M* = maneuver, *I* = impact.

[d] Using radius of moon = 1738.0 (recording accuracy of 0.025 sec). Note: Orbit used for maneuver calculations is underlined.

§ The material relating to Table 4 and Figs. 8 and 9 is derived from PD-30 (JPL Internal Document) by K. R. Young.

Table 3 Maneuver evaluation

Commanded maneuver	Ranger 6			Ranger 7		
Roll, deg	−12.01			5.56		
Pitch, deg	−71.06			−86.80		
ΔVelocity, m/sec	41.27			29.89		
Duration, sec	67.0			49.0		
Time, hr	Launch + 17.1			Launch + 17.5		
Over-all errors	$\Delta B\cdot T$, km	$\Delta B\cdot R$, km	ΔT, sec	$\Delta B\cdot T$, km	$\Delta B\cdot R$, km	ΔT, sec
OD(in-best)	+12.4	−78.7	−14.5	−6.0	−13.2	+11.8
Maneuver	−1.2	+39.8	+20.5	+22.9	−3.6	+6.2
Over-all	+11.2	−38.9	+6.0	+16.9	−16.8	+18.0
ΔLatitude	0.80° ≈ 24.0 km	27 km = 16 miles on lunar surface		0.30° ≈ 9.0 km	13 km = 8 miles on lunar surface	
ΔLongitude	0.45° ≈ 12.0 km			0.32° ≈ 10 km		

phases of a Ranger mission. The limiting error sources are also discussed.

The results presented are based on a conservative effective weighting sigma of 0.03 m/sec for doppler and 0.18° for angles for data sampled once a minute. Only DSIF tracking data are considered, and practical limits of station operation are recognized. These limits include the following:

1) All stations acquire two-way doppler lock 5 min after rise (i.e., after 5° elevation and $-100° \leq HA \leq 100°$).

2) Only one DSIF station obtains two-way doppler at a time.

3) The maximum allowable angular rate for the DSIF antennas is 0.7°/sec. The only time this constraint is in danger of being violated for Ranger is during the first pass over South Africa.

Station locations, $GM_\oplus$ and $GM_\leftmoon$ (universal gravitational constant times the mass of the earth and moon) were included in the solution vector, with the following uncertainties:

$$\sigma_{GM_\oplus} = 4 \text{ km}^3/\text{sec}^2 = (1 \times 10^{-5})GM_\oplus$$

$$\sigma_{GM_\leftmoon} = 5 \text{ km}^3/\text{sec}^2 = (1 \times 10^{-3})GM_\leftmoon$$

Station locations are as follow: $\sigma_{\text{radius}} = 60$ m, $\sigma_{\text{longitude}} = 0.001° \approx 110$ m, and $\sigma_{\text{latitude}} = 0.001° \approx 110$ m.

The premidcourse *OD* accuracies are a strong function of the time of the maneuver and the injection geometry with respect to the DSIF tracking stations. Two cases are considered, namely, supporting an early maneuver commanded from the DSIF station in South Africa and supporting a maneuver commanded from the DSIF station at Goldstone.

The early maneuver support capability is illustrated in Fig. 8. The SMAA varies from 10 to 100 km, and thus, the Ranger project requirement of 150 km is always satisfied. The order-of-magnitude range in the SMAA is caused by the quantity of data used in the orbit calculation as well as the geometry of the spacecraft relative to the tracking stations. The data quantity varies for two reasons. First, the restriction that no tracking data can be used which are obtained within 7 hr from the end of the South African pass means that the time of the last data point varies from $L + 270$ min to $L + 500$ min. The earlier times correspond to uprange injections at a 114° launch azimuth and the later times to a downrange injection at 90° launch azimuth. The launch azimuth produces the weaker variation of the two variables. The second item affecting data quantity is also related to view periods of the station. South Africa may have two view periods within the first 16 hr after launch. As the spacecraft proceeds along an earth track, it may rise over South Africa, then set as it proceeds in an easterly direction toward Australia. The spacecraft will then rise again over South Africa, as it changes its direction in the earth track and starts its westerly motion for the remainder of the trip. If the injection location is far enough downrange, and if the launch azimuth is less than 102°, the "first" pass may be nonexistent or too short for South Africa to acquire two-way doppler. Early tracking data are generally the most important data in determining an orbit because of the relatively rapid rate of change of direction of the observations. The effect of this data loss is illustrated in Fig. 8 by the change in the SMAA across the boundary that divides the region that has a first pass over South Africa of less than 5 min (i.e., no doppler data are obtained) from the longer passes in which doppler data are obtained.

Another discontinuity exists at the extreme uprange injection locations for launch azimuths greater than 107°. The earth track for these injections bends back toward the West before Australia is able to acquire two-way doppler. This means that these orbits are determined by data from only one station (South Africa), and the orbit does not benefit from the relative geometry of the two stations.

The Goldstone maneuver support capability is also illustrated in Fig. 8. The time of the last data point varies from $L + 13$ to $L + 20$ hr. Although the same discontinuities exist for this case as for the previous case, their effects are tempered by the larger quantity of tracking data plus data from one more station. The SMAA ranges from 10 to 70 km, the worse case being in the region for which no early data are available from South Africa.

The *OD* capability for the previous situations is well within the Ranger project requirements. However, as demonstrated by the examples cited for Ranger VI, the main inflight *OD* problem in meeting the requirements of the project is uncover-

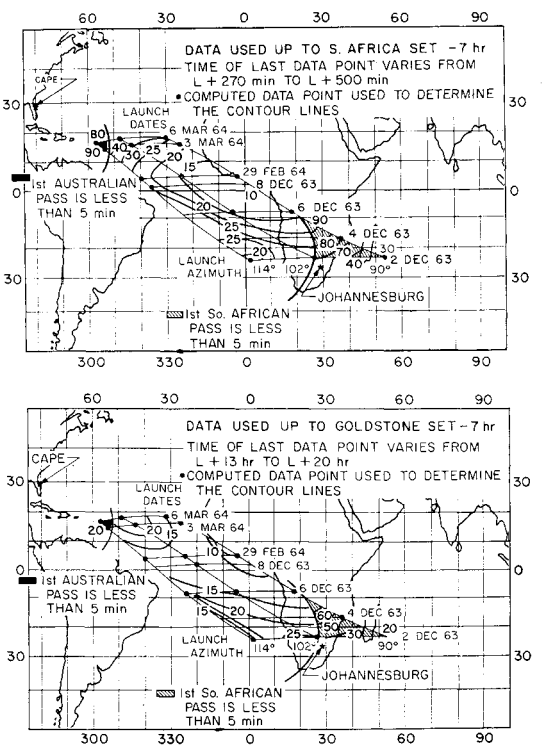

Fig. 8 Ranger premidcourse tracking accuracies.

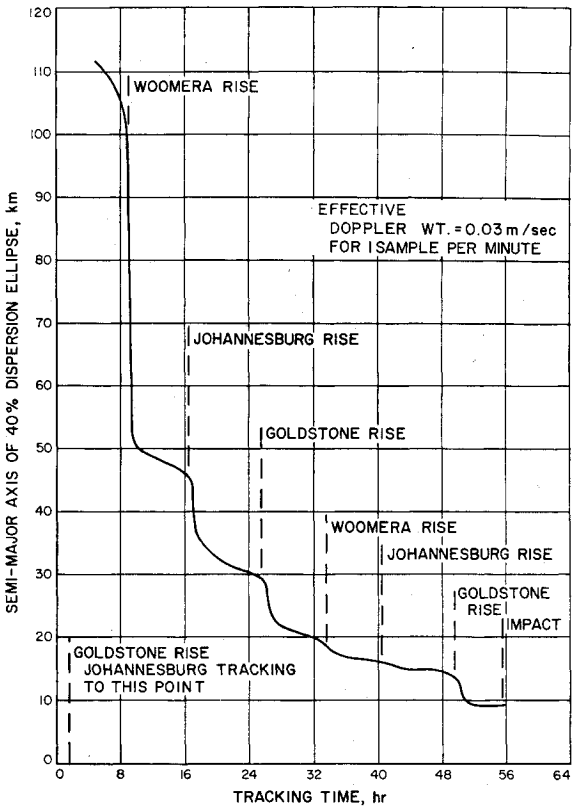

Fig. 9 Dispersion vs tracking time, postmidcourse.

ing inconsistencies in the data as opposed to processing every last datum in order to overcome the random noise on the tracking data. These real-time data consistency checks are best made by comparing the data from one tracking station against an orbit determined by tracking data from other stations.

The final postmidcourse *OD* accuracies are relatively invariant for the class of trajectories used for Ranger. An example of these postmidcourse accuracies is shown in Fig. 9. The spacecraft position was assumed known to 10 km and the velocity to 1 m/sec immediately after the maneuver. This requires discarding most of the information obtained through premidcourse tracking of the spacecraft, and thus, the postmidcourse *OD* process is less sensitive to any anomalies that exist in the premidcourse tracking data. Notice that a sharp decrease in the SMAA occurs each time a different station starts tracking until the SMAA approaches a minimum of 9 km, 4 hr before lunar encounter. The limiting error source in this case is the uncertainty in the location of the tracking stations.

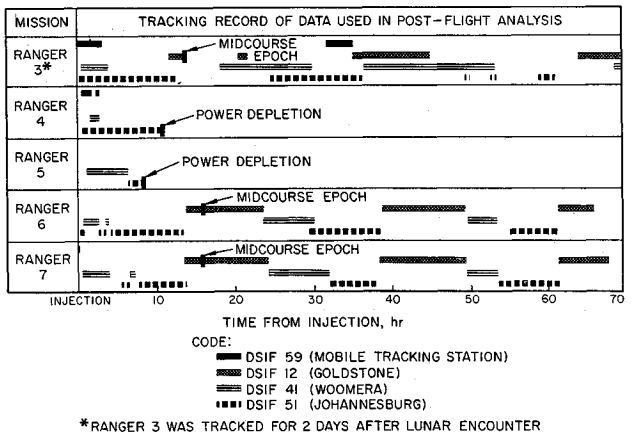

Fig. 10 Tracking record, Rangers III–VII.

The effect of including physical constants in the solution vector is illustrated in Table 4, which presents the results of estimating the spacecraft orbital elements along with station locations $GM_\oplus$ and $GM_\leftmoon$ in different combinations. The principal parameters limiting the SMAA near lunar encounter are the uncertainties in the location of the tracking stations. Estimating the orbital elements by themselves or in combination with $GM_\oplus$ and/or $GM_\leftmoon$ limits the SMAA to 4 km, but the inclusion of station locations in any of these runs raises it to 9 km.

The definition of the *B*-plane is such that estimating $GM_\leftmoon$ has no first-order effect on the *B*-plane statistics. These statistics essentially represent a mapping of the uncertainties in the direction of the hyperbolic excess velocity vector of the spacecraft with respect to the moon. The direction of the hyperbolic excess velocity vector is essentially not a function of the mass of moon. However, the uncertainty of the mass of the moon does influence the time-of-flight uncertainty. Notice that the velocity of light is not included in the solution vector. This is because the light second is considered the basic unit of length in the "radio world."

The postmidcourse uncertainties, quoted in this section, essentially assume that position and velocity information are not carried across the maneuver. The postflight SMAA for Rangers VI and VII was 2 km in the *B*-plane, which is equivalent to 1.2 km on the lunar surface. This smaller SMAA (i.e., 2 km as compared to 9 km) is realized when the pre- and postmidcourse tracking data are processed under the following two constraints: 1) that the knowledge of the spacecraft position is only mildly affected by the midcourse maneuver and 2) that the earth-moon distance and the masses of the earth and the moon are such that the earth-moon period remains fixed. That is, the period of moon about the earth is known to far greater precision than any of these three variables.

Physical Constant Solutions

A data coverage chart is shown in Fig. 10. It appears that Ranger III (launched January 1962) had very good coverage; however, the data accumulated at Woomera, station 41, and Johannesburg, station 51, were only angular data, and the doppler data (from Goldstone, station 12, and the mobile tracker in South Africa) which are by far the most powerful data sources, did not match the quality experienced on Rangers VI and VII. Ranger IV (launched April 1962) suffered power depletion after approximately 8 hr, but it had the added feature of doppler capability at Woomera. Rangers VI (launched January 1964) and VII (launched July 1964) had virtually the same coverage. Extremely good data were acquired at Goldstone, and both Woomera and South Africa obtained good doopler data. These are the best deep-space

Table 4 Effect of physical constants on target statistics

Parameters[a], estimated	a, km[b]	θ, deg[b]	σ_T, sec[b]	a, km[c]
P, V	3.8	94.9	0.07	11.5
$P, V, GM_\leftmoon$	3.8	94.9	0.09	11.5
$P, V, GM_\oplus$	4.0	95.2	0.07	11.6
$P, V, GM_\leftmoon, GM_\oplus$	4.0	95.2	0.10	11.6
P, V, SL	8.8	96.6	0.08	16.3
$P, V, GM_\oplus, SL$	8.9	96.5	0.08	16.4
$P, V, GM_\leftmoon, SL$	8.8	96.6	0.10	16.3
$P, V, GM_\leftmoon, GM_\oplus, SL$	8.9	96.5	0.11	16.4

[a] P = position, V = velocity, SL = station location.
[b] Results after tracking to impact (52.5 hr): a = semimajor axis of 40% dispersion ellipse in the B plane (the semiminor axis was equal to 0.4 km in all cases); θ = the orientation angle of semimajor axis measured counterclockwise from the T axis; and σ_T = one sigma on time of flight. Statistics are based on an effective 2-way doppler weighting sigma of 0.03 m/sec for 1 sample/min. A priori sigmas were $GM_\oplus$ = 4.0 km³/sec², $GM_\leftmoon$ = 5.0 km³/sec², station radius = 60.0 m, and latitude and longitude = 0.001°.
[c] Results after tracking 35½ hrs.

probe data ever acquired. Mariner II data coverage is shown in Fig. 11. Its data came periodically from Goldstone, which was using a rubidium transmitter frequency standard for the first time.

A typical fit to the data is shown in Fig. 12. The discrete points are the residuals or the difference between the observed data and that value calculated in the theoretical model. This frame of data covers the last 6 hr prior to lunar impact and is part of a complete fit to all of the Ranger VII data. Note the remarkable absence of biases even in the last few hours, when the moon's gravitational effect is so predominant. Also evident here is the effect of the stability of the transmitter using the rubidium standard. The noise increase is caused by transmitter drift during the signal travel time. The visible noise on the rubidium data is 0.0088 cps or approximately 0.0014 m/sec on a 1-point/min sample rate. Figure 13 shows the increase in noise on the doppler as a function of range caused by transmitter drift. These data are from South Africa, station 51, which does not have the rubidium standard. A detailed analysis of doppler-data residuals is available in Refs. 2 and 3. Many effects can be seen in the doppler residuals such as the one just mentioned. Therefore, a flexible weighting model is required to weight each data point properly to account for its own particular noise characteristics. Table 5 lists the six noise sources that contribute to the final weight for two-way doppler. They include 1) computer error, 2) cycle roundoff, 3) transmitter drift, 4) cycle drop-out or add-in, 5) refraction, and 6) spacecraft tumbling. The three columns adjoining each noise source are 1) a sensitivity coefficient g, 2) a 1-sigma uncertainty on the noise source s, and 3) a correction period T_L. The various elements are then accumulated for each data point as shown by the formula at the bottom of the table, and this effective weight is assigned to the data point.

The estimation of physical constants is accomplished with the JPL orbit determination digital computer program[4] that does a weighted least-squares fit to as many as 20 parameters simultaneously. For example, the probes' six orbital elements, $GM_{\oplus}$, $GM_{\mathbb{C}}$, the lunar-scale factor, a solar pressure coefficient, and three components of station location for three stations were all estimated at once with Ranger VI data.[2] This program has been very extensively tested and is the same program used in flight operations, where it so dramatically proved itself with the close agreement to the television cam-

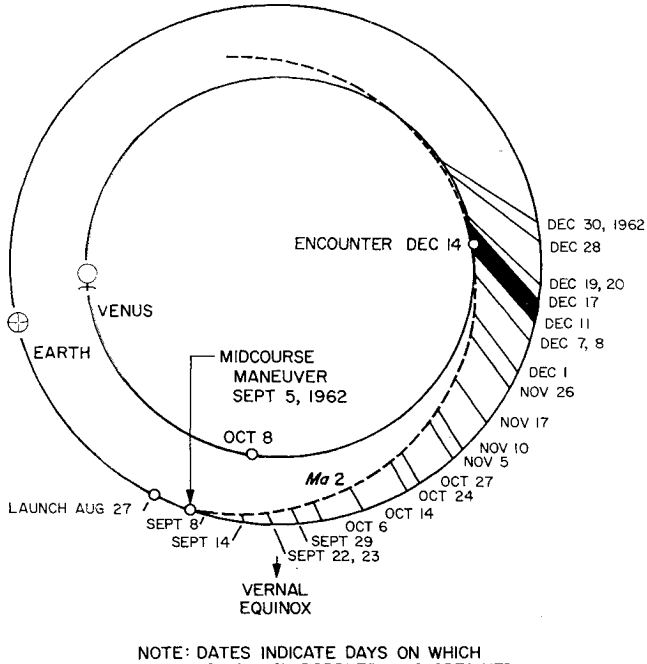

NOTE: DATES INDICATE DAYS ON WHICH TWO-WAY DOPPLER WAS OBTAINED

Fig. 11 Tracking pattern on Mariner II.

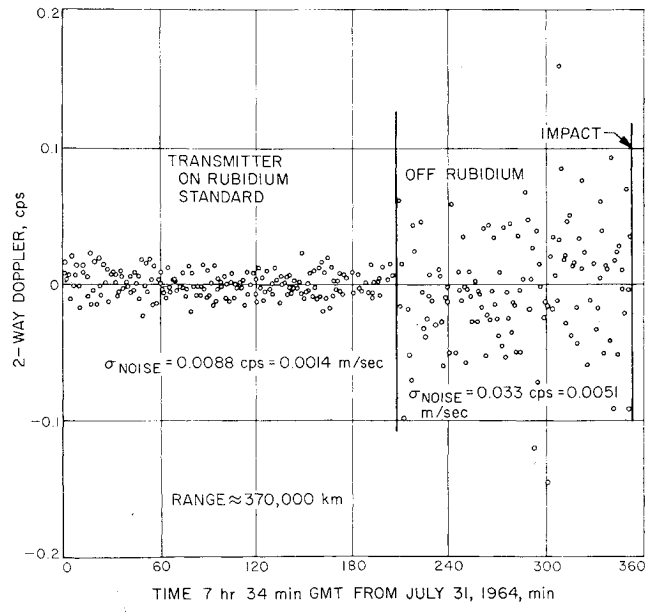

Fig. 12 Goldstone residuals at impact, Ranger VII.

era results. The solutions given below are the results of estimating all of the parameters simultaneously over all of the data for that particular mission. The postflight analysis of the tracking data used a priori uncertainties for the orbital elements and the physical constants which were much larger than final solution statistics. Therefore, the resultant statistics reflect the ability of the tracking data to estimate that parameter.

The station locations can be estimated quite well in two coordinates and very poorly in the third. Figure 14 shows the coordinate system that best suits station location estimation using space probe data. The x_1 axis is normal to the earth's spin axis passing through the station in the station meridian plane. The x_2 coordinate is similar to longitude. It is normal to x_1 and to the earth's spin axis. The third coordinate x_3 is parallel to the earth's spin axis. The x_1 and x_2 components are well determined from the tracking data, whereas x_3 is only partially determined (Ref. 5 gives a detailed analysis). In general, when horizon-to-horizon tracking is available, x_1 can be determined to within 10 m, and the differences in longitude between two stations can be obtained to 20 m.

Table 6 displays the station location results from Ranger VI, Ranger VII, and Mariner II as deviations from a "best" land survey. Note the consistency in the differences. Station 12, Goldstone, has the best estimates since it has the rubidium standard and consequently has been allowed to accumulate much more tracking data (horizon-to-horizon track). Note that the statistics on x_1 at Goldstone are a factor of three below the best land surveys and that the statistics in the differences in longitude are also below land surveys. With rubidium standards at Woomera and South Africa in the near future, these stations will be determined as well as Goldstone, and an improved world survey reference will be available.

Table 7 shows the $GM_{\oplus}$ solutions. All estimates seem to lie consistently below the nominal value (398603.2) at approximately 398601.0 ± 1. Rangers VI and VII are very consistent and have a factor of four smaller uncertainty than other present estimates.

Table 7 also shows the $GM_{\mathbb{C}}$ estimates and statistics.

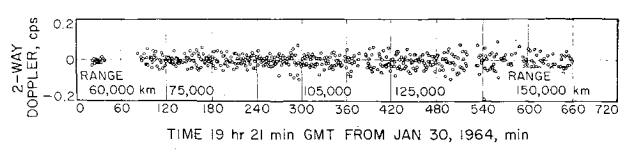

Fig. 13 Doppler noise growth, South Africa, Ranger VI.

Table 5 Data weighting[a]

Error source	Early doppler, range ≈ 55,000 km				Late doppler (near lunar encounter), range ≈ 383,000 km			
	g_i^2	s_i^2	Correlation width, sec	i^2 (cycles)^2	g_i^2	s_i^2	Correlation width, sec	σ_i^2 (cycles)^2
Computing error	1	1.1×10^{-5}	36,000	65.6×10^{-4}	1	1.1×10^{-5}	36,000	65.6×10^{-4}
Rounding error	2.78×10^{-4}	0.16	1	0.47×10^{-4}	2.78×10^{-4}	0.16	1	0.47×10^{-4}
Oscillator drift rate	0.0189	0.41×10^{-2}	600	$(VCO)_T$	0.917	$(0.41 \times 10^{-2})_{VCO_T}$	600	$(376.1 \times 10^{-4})_{VCO_T}$
				7.76×10^{-4}		$(0.41 \times 10^{-6})_{VCO_R}$		$(0.03761 \times 10^{-4})_{VCO_R}$
Dropped or added cycles	5.56×10^{-3}	0.96	1	5.43×10^{-4}	5.56×10^{-3}	0.96	1	5.44×10^{-4}
Refraction correction	1.11×10^{-6}[b]	0.04	1,000	0.0007×10^{-4}	3.92×10^{-6}[c]	0.04	1,000	0.026×10^{-4}
Spacecraft tumbling		Zero for Ranger 6				Zero for Ranger 6		
Total	$\sum_{i=1}^{6} \sigma_i^2 = 79.24 \times 10^{-4}$ $\sigma = 0.089$				$\sum_{i=1}^{6} \sigma_i^2 = (446.6 \times 10^{-4})_{VCO_T} = (71.5 \times 10^{-4})_{VCO_R}$ $\sigma = (0.211)_{VCO_T} = (0.085)_{VCO_R}$			

[a] Sample rate = count time = 60 sec; T = not on rubidium standard; R = on rubidium standard; and $\sigma = \left[\sum_{i=1}^{6} \sigma_i^2\right]^{1/2} = \left[\sum_{i=1}^{6} g_i^2 s_i^2 \max\left\{1, \frac{T_{corr}}{T_{sample}}\right\}\right]^{1/2}$

[b] Elevation = 45°; elevation rate = 0.0028°/sec.

[c] Elevation = 36°; elevation rate = 0.0030°/sec.

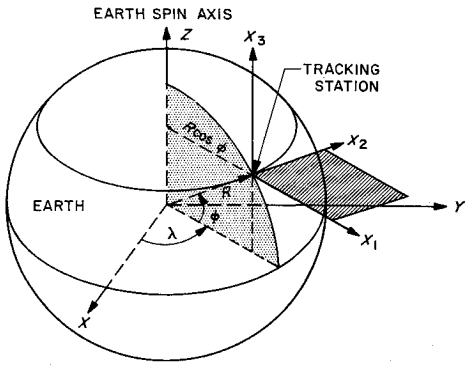

Fig. 14 Station coordinate system.

Mariner II was the first to determine this constant a magnitude better than the nominally accepted value. The 28-day periodic effect of the moon in Mariner II's cruise phase data was very dramatic, and a solution[7] was easily obtained. In contrast, Ranger VI and VII estimates were derived strictly from the moon's gravitational effect in the last few hours before impact. The complete agreement with Mariner II is very encouraging and gives the estimate strong additional support.

Another constant that can be obtained from the Ranger VI and VII flights is the lunar radius ($R\mathbb{C}$) at the impact points. This estimate is directly dependent on the recording of impact time. The accuracy of the recording is ±0.025 sec which reflects into a 0.05-km variation in $R\mathbb{C}$. However, the overall orbit determination accuracy is 0.15 sec and implies a $R\mathbb{C}$ uncertainty of 0.3 km. A time residual in both Rangers VI and VII caused a decrease of approximately 3.1 and 2.4 km, respectively, to fit impact time, when ACIC Lunar Charts[8] were used for elevations at the impact points and 3.6 and 4.4 km, respectively, when U. S. Army Lunar Maps[9] were used.

Further Applications of EBRG

Earth-based radio tracking is being used for the Mariner IV (Mars) and will be used for the Surveyor and the Apollo missions. The Mariner IV trajectories have been designed, so that Mars will occult the probe. This will provide valuable information about the Martian atmosphere and the radius of Mars by measuring the change in the doppler signal, as it passes through the Martian atmosphere. In addition, the Mariner IV tracking data will be used to determine the Astronomical Unit (AU) (mean earth-sun distance) and the mass of Mars. For the Surveyor mission, EBRG may also be

Table 6 Station location estimates

Mission	Coordinates[a]					
	Off spin axis		Longitude		Longitude difference	
	X_1	σ_{X_1}	X_2	σ_{X_2}	ΔX_2	$\sigma_{\Delta X_2}$
	Goldstone				Woomera	
Land survey	0	30	0	30	0	37
Mariner 2	−24	30	9	30	...	...
Ranger 6	−36	10	−18	32	−131	22
Ranger 7	−35	9	1	31	140	23
	Woomera				Johannesburg	
Land survey	0	30	0	30	0	37
Ranger 6	88	38	113	39	154	22
Ranger 7	65	37	141	37	167	25
	Johannesburg				Goldstone	
Land survey	0	30	0	30	0	37
Ranger 6	−33	19	−41	36	−23	19
Ranger 7	−16	21	−26	31	−27	18

[a] All units are meters; X_1, X_2, and ΔX_2 are differences of mission result and land survey.

Table 7 $GM_{\oplus}$ and $GM_{\mathbb{C}}$ with probable errors[a]

Source	Value, km³/sec²	Standard deviation, km³/sec²	Tracking time, hr
	GM_{Earth} estimates = $GM_{\oplus}$		
Nominal JPL[b]	398603.20	±4.0	
Ranger 3	398600.49	±4.1	96
Ranger 4	398601.87	±13.3	8
Ranger 5	398599.20	±13.2	8
Ranger VI	398600.61	±1.1	65
Ranger VII	398601.28	±1.5	68
	GM_{Moon} estimates = $GM_{\mathbb{C}}$		
Nominal JPL (prior to Mariner 1962)	4900.7589	±5.0	...
Nominal JPL[b,c] (after Mariner 1962)	4902.7779	±0.3	...
Ranger VI	4902.6182	±0.14	65
Ranger VII	4902.5801	±0.17	68

[a] Nominal values shown in these figures are taken from Ref. 6 and uncertainties are quoted as probable errors.
[b] Value set by Symposium 21, Internation Astronomical Union, Paris, 1963.
[c] Cruise data taken during Mariner-Venus, 1962.

employed to back up the onboard sensor used to initiate the terminal descent sequence. EBRG is also emerging as the primary guidance method for the major portion of the Apollo mission.

The physical properties of the atmosphere of Mars are of great interest to astronomers and to the engineers who are planning to land instrumented spacecraft on the surface of the planet. This latter undertaking requires an improved knowledge of both the density of the atmosphere of Mars at the surface and its variation with altitude. Reference 10 describes how this objective is to be realized with Mariner IV by observing the frequency changes of the spacecraft doppler data caused by the signal traveling through the atmosphere of Mars prior to occultation by the planet.

Radio tracking of the spacecraft within the solar system is a source of powerful new types of measurements previously unavailable to workers in celestial mechanics. The combination of radio tracking data, radar "bounce" data, and optical data may effect an improvement in our knowledge of the planetary ephemerides and the solar physical constants needed to accomplish the guidance of a probe from the earth to a selected area on a planet such as Mars by use of EBRG alone.

Summary

The capability of EBRG has been dramatically demonstrated by the successes of Rangers VI and VII impacting the lunar surface only 27 and 13 km, respectively, from the aim point. The orbit determination accuracies available from DSIF tracking data can easily satisfy the requirements of the Ranger project; however, the main task is to detect irregularities in the tracking data in near real-time.

Postflight processing of the tracking data has provided a best-estimate orbit of sufficient quality to be used as a standard in determining the accuracy of real-time orbit determination estimates and the execution errors of the midcourse maneuver.

Significant determinations of certain physical constants have been another product of this postflight analysis of the tracking data. An improvement of one order of magnitude has been effected in the knowledge of the mass of the moon and of a factor of four for the earth. Information was also obtained on the tracking station locations at the Ranger VI and VII impact points. Station locations can be determined to within 10 m in the radial direction normal to the earth's spin axis, and differences in the longitude between stations can be calculated to within 20 m. The radius of the moon at the Ranger VI and VII impact points was determined to ±0.3 km, and in both cases, it was found to be approximately 3 km less than the previously accepted value.

EBRG will be used for the Mariner IV, Surveyor, and the Apollo missions. In the case of Mariner IV, the trajectory has been designed so that Mars will occult the probe. This will provide valuable information about the Martian atmosphere and the radius of Mars by measuring the change in the doppler signal, as it passes through the Martian atmosphere.

References

[1] Bayley, W. H. and Rechtin, E., "System capabilities and development schedule of the DSIF, 1964–1968," Tech. Memo. 33-83, Revision 1, Jet Propulsion Lab., Pasadena, Calif. (April 24, 1964).

[2] Sjogren, W. L., Curkendall, D. W., Hamilton, T. W., Kirhofer, W. E., Liu, A. S., Trask, D. W., Winneberger, R. A., and Wollenhaupt, W. R., "The ranger VI flight path and its determination from tracking data," TR 32-605, Jet Propulsion Lab. Pasadena, Calif. (December 1964).

[3] Wollenhaupt, W. R., Trask, D. W., Sjogren, W. L., Piaggi, E. G., Curkendall, D. W., Winneberger, R. A., Liu, A. S., and Berman, A. L., "The Ranger VII flight path and its determination from tracking data," TR 32-694, Jet Propulsion Lab., Pasadena, Calif. (December 1964).

[4] Warner, M. R., Nead, M. W., and Hudson, R. H., "The orbit determination program of the Jet Propulsion Laboratory," Tech. Memo. 33-168, Jet Propulsion Lab., Pasadena, Calif. (March 18, 1964).

[5] Cain, D. L. and Hamilton, T. W., "Determination of tracking station locations by doppler and range measurements to an Earth satellite," TR 32-534, Jet Propulsion Lab., Pasadena, Calif. (February 1, 1964).

[6] Clarke, V. C., Jr., "Constants and related data for use in trajectory calculations as adopted by the AD HOC NASA standard constants committee," TR 32-607, Jet Propulsion Lab., Pasadena, Calif. (March 6, 1964).

[7] Anderson, J. D., Null, G. W., and Thornton, C. T., "The evaluation of certain astronautical constants from the radio tracking of Mariner II," *AIAA Progress in Astronautics and Aeronautics: Celestial Mechanics and Astrodynamics*, edited by Victor G. Szebehely (Academic Press Inc., New York, 1964), Vol. 14.

[8] "Lunar charts (both at 1:1,000,000 scale)," Aeronautical Chart and Information Center, U. S. Air Force, LAC 60 (September, 1962); also LAC 76 (April, 1964).

[9] "Topographic lunar map, 1:5,000,000," Army Map Service Corps of Engineers, Washington, D. C., edition 2-AMS (June 1964).

[10] Kliore, A., Cain, D. L., and Hamilton, T. W., "Determination of some physical properties of the atmosphere of Mars from changes in the doppler signal of a spacecraft on an Earth-occultation trajectory," TR 32-674, Jet Propulsion Lab., Pasadena, Calif. (October 1964).